FAR-FIELD OTR AND ODR IMAGES PRODUCED BY 7-GEV ELECTRON BEAMS AT APS*

A.H. Lumpkin, B.X.Yang, W.J. Berg, N.S. Sereno, and C.-Y. Yao, Argonne Accelerator Institute,
Argonne National Laboratory, Argonne, IL 60439, U.S.A.
D.W. Rule, Carderock Division, NSWC, West Bethesda, MD 20817, U.S.A.

Abstract

We have investigated the angular distribution patterns (far-field focus) of optical transition radiation (OTR) and optical diffraction radiation (ODR) generated by 7-GeV electron beams passing through and near an Al metal plane, respectively. The 70-μrad opening angles of the OTR patterns provide calibration factors for the system. Effects of the upstream quadrupole focusing strength on the patterns as well as polarization effects were observed. The OTR data are compared to an existing OTR single-foil model, while ODR profile results are compared to expressions for single-edge diffraction. ODR was studied with impact parameters of about 1.25 mm, close to the gamma lambda–bar value of 1.4 mm for 628-nm radiation. We expect angle-pointing information along the x axis parallel to the mirror edge is available from the single-lobe ODR data as well as divergence information at the sub-100-μrad level. Experimental and model results will be presented.

INTRODUCTION

Our interest in characterizing the 7-GeV beam in the transport line to the storage ring has been ongoing since the beginning of our top-up operations of the Advanced Photon Source (APS) facility. In this mode we inject 2-3 nC every two minutes into the standard fill pattern (24 singlets evenly spaced by 153 ns). Although the trajectory is tracked by the rf beam position monitors (BPMs), there is no nonintercepting (NI) beam profile diagnostic available in this transport line. We initially performed a series of studies on optical diffraction radiation (ODR) as a potential NI beam-size monitor as referenced to optical transition radiation (OTR) measurements [1,2]. We used focus-at-the-object or near-field imaging optics and established that the orthogonal polarization component of ODR has the beam size sensitivity that we needed for the transport line with its 1200- to 2500-μm rms sizes in the x-plane [2]. We have now investigated the angular distribution patterns (focus at infinity or far-field focus) of optical transition radiation (OTR) and optical diffraction radiation (ODR) generated by 7-GeV electron beams passing through and near an Al metal plane, respectively, at the same test station. By using two different lattice setups in the synchrotron for a different base emittance and by varying an upstream quadrupole in the BTX transport line, we have extracted a range of beam sizes and now preliminary beam-divergence information from

the images. Under the assumption that we have identified an x-waist condition at our station, we have extracted a preliminary emittance measurement from the OTR and then assessed the complementary ODR results. We have also looked at the trajectory angle data with both far-field OTR and ODR and found the ODR θ_x centroid tracks the OTR θ_x centroid well. Since we only used a single metal plane inserted vertically above the beam axis, we observed only single-lobe ODR angular distributions (unlike the annular OTR angular distributions) as expected.

EXPERIMENTAL BACKGROUND

The tests were performed at the APS facility which includes an injector complex with two rf thermionic cathode (TC) guns for injecting an S-band linac that typically accelerates the beam to 325 MeV, the particle accumulator ring (PAR), the booster synchrotron that ramps the energy from 0.325 to 7 GeV in 220 ms, a booster-to-storage-ring transport line (BTS), and the 7-GeV storage ring (SR) as shown previously [1]. The tests were performed in the booster extraction line (BTX) where energizing a dipole sends the beam into this spur line that ends in a beam dump. The setup includes the upstream corrector magnets, quadrupoles, and this dipole, and then an rf BPM (single-plane striplines only), the OTR/ODR imaging station, a localized beam-loss monitor based on a Cherenkov radiation detector, the Chromox beam-profiling screen, and the beam dump, as schematically shown in Fig. 1. The rf BPM located just before the ODR station was a single-plane device, and it was initially oriented to monitor vertical beam position during impact-parameter studies. The BPM is presently rotated 90 degrees to provide direct, complementary horizontal beam position monitoring. The BPM and downstream flag were used to verify the trajectory in the setup of the beam steering.

The ODR converter is a polished Al blade/mirror that is 1.5 mm thick, 30 mm wide, 30 mm tall, and is mounted with its surface normal at 45 degrees to the beam direction on a stepper assembly. The assembly provides vertical positioning with an overall accuracy of ± 10 μm over a span of 27.5 mm. The OTR and ODR were directed by turning mirrors and relay optics to a Sony Model XC-ES50 CCD camera located 1.8 m from the source. With the addition of the transport optics, which allowed remote switching between near-field and far-field imaging, a careful survey and laser alignment procedure was required. The upstream beam pipe section was removed to allow the survey transit and telescope to be
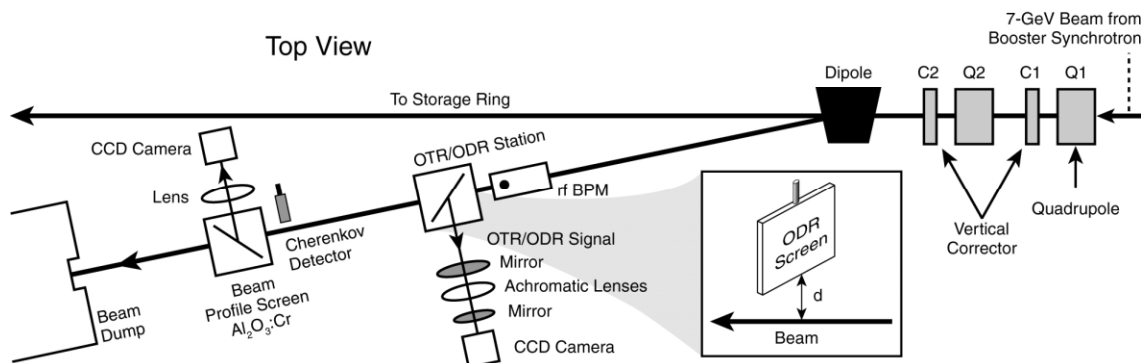
Figure 1: A schematic of the BTX test area showing the upstream quadrupoles and corrector magnets, the dipole, the rf BPM, the OTR/ODR station, the optics with camera, the Cherenkov detector, the Chromox beam-profiling screen, and the beam dump.

located on the beamline axis. This alignment proved to be critical to the successful far-field imaging and also resulted in improved total signal collected by the optics. We still suspect the largest horizontal plane beam sizes may have resulted in incomplete signal collection over angle space. The near-field magnification resulted in calibration factors of 60 μm per pixel in x and 46 μm pixel in y. The far-field magnification resulted in angle calibration factors of 2.6 μrad per pixel in θ_x and 2.0 μrad per pixel in θ_y. Two 6-position filter wheels were used just in front of the camera to select neutral density (ND) filters, bandpass filters, or two polarizers oriented at 90 degrees to each other. The OTR and ODR images were recorded with a Datacube MV200 video digitizer for both online and offline image analyses. In these more recent experiments, the rf BPM was rotated to monitor horizontal position just before the ODR screen, and the charge was monitored by an upstream current monitor.

OTR RESULTS

The experiments were usually initiated by verifying the OTR-deduced spot sizes and centering of the beam on the screen centerline and the downstream camera target coordinates. For a quadrupole setting of AQ2=34 A we observed a beam spot with σ_x = 2460 μm, σ_y = 220 μm, and an asymmetry of 11 for the ratio of σ_x/σ_y. With a beam energy of 7 GeV the expected opening angle would be 73 μrad. In Fig. 2 we show the horizontal polarization component (upper) and vertical polarization component (lower) of the angular distribution pattern for AQ2=29.3 A. The horizontal beam size is now 1290 μm, and the beam divergence, as expected, is large enough in convolution to fill in the central minimum. In Fig. 3 we show the horizontal profile (I_{par}) at the left. In addition, $\sigma_{y'}$ information is available in Fig. 3 where the very deep central minimum is observed in the vertical profile of the vertically polarized image. A reasonable quantitative estimate of the beam x divergence can be done by comparing the experiment to the analytical results shown in Fig. 4 for the case with x and y divergences of 50 and 10 μrad, respectively. The $\sigma_{x'}$ experimental result is close to the 50-μrad case based on the similar 30% dip in intensity at θ_x = 0. The $\sigma_{y'}$ value is close to a 10-μrad

value based on calculations performed for divergences of 3, 10, and 20 μrad. We show the 10-μrad case with a 50-μrad value used for the orthogonal component. This latter value causes an increase in the I_{perp} component, but the central minimum of the I_{par} component is still about 10% of the two peaks' intensities, similar to the data.

Based on our quadrupole-scan results, there is an approximate x-beam waist at this 29.3-A setting so a direct product of the observed rms x-beam size and the x divergence is equal to the geometric emittance, in this
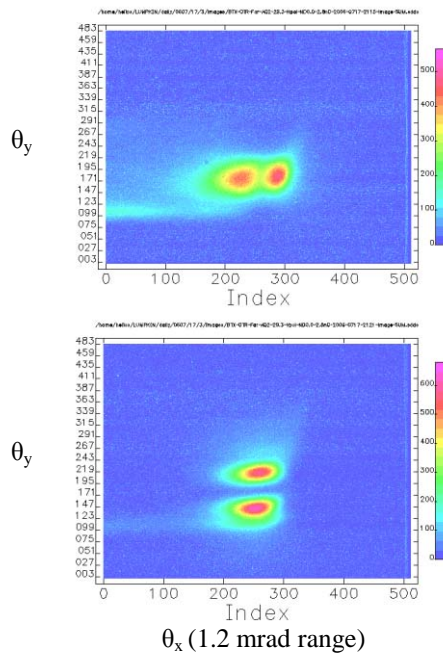

θ_x (1.2 mrad range)

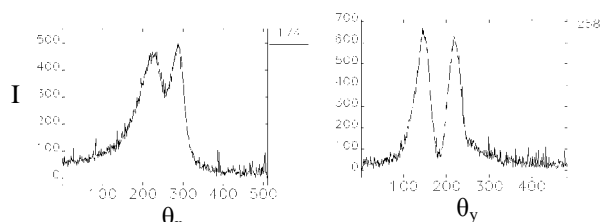Figure 2: Horizontally polarized OTR image (upper) and vertically polarized OTR image (lower) for AQ2=29.3 A.

Figure 3: Horizontal profile (left) and vertical profile (right) from the respective polarized images in Fig. 2.
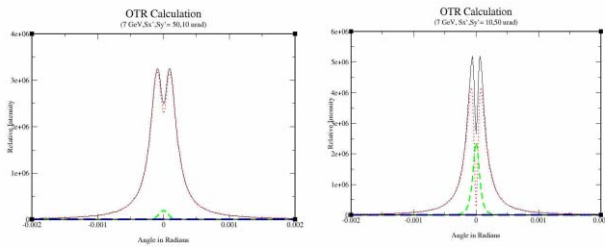
06 Instrumentation, Controls, Feedback & Operational Aspects

T03 Beam Diagnostics and Instrumentation

Figure 4: Analytical model calculations for 7-GeV energy and x and y beam divergences of 50 and 10 µrad, respectively, at the left and the reverse at the right. The total intensity (black), the I_{par} component intensity (red), and the I_{perp} component intensity (green) versus angle are shown.

case, 1290 µm × 50 µrad = 65 nm rad. The simulated low-emittance lattice value for the booster in the 92-nm lattice, when run at a negative-momentum offset of -0.8%, is 62 nm rad [3], so the values are in good agreement. Since this lattice also has horizontal dispersion at this location, we still need to subtract that contribution out in quadrature from the observed OTR x profile width. An independent experimental result of 77 nm rad was deduced from a quadrupole scan data set taken in the adjacent BTS line. This latter larger result also needs the dispersion contribution addressed and may have also been limited by the inherent poorer resolution of the Chromox screen used in the imaging.

ODR RESULTS

The ODR results with a single metal screen above the beam are not visually as striking as the OTR images. The near-field x profile using the vertical polarization component has a σ_x of 1590 µm compared to the OTR σ_x of 1290 µm. This 25% difference was seen in our lookup table [2] for the AQ2=29.3A setting and an impact parameter of 1.25 mm. The ODR vertically polarized far-field image is shown in Fig. 5. As a trial, we take the horizontal angle cut though this image and obtain the profile in the right of Fig. 5. The profile has a size of ~156 µrad (FWHM). Muto et al. [4] previously reported observations of unpolarized ODR far-field angular distributions and compared them to theory, neglecting beam-divergence effects. Actual calculations of the ODR profiles with the beam divergences convolved are needed to evaluate sensitivity to beam divergence for diagnostic purposes in this regime. In Fig. 6 we show the expected vertically polarized ODR profiles for divergences of 1, 25, and 50 µrad. The latter case has a width of 164 µrad (FWHM) in good agreement with our experiment. Although there is direct sensitivity in both polarizations, the horizontal polarization component was too weak in signal for our conditions of low charge. We do note that as we changed the quadrupole settings and the upstream dipole, the ODR and OTR θ_x centroids tracked the beam trajectory directly. So the x angle can be monitored with the far-field optics and a vertically inserted single metal plane just as the near-field images tracked the x position.
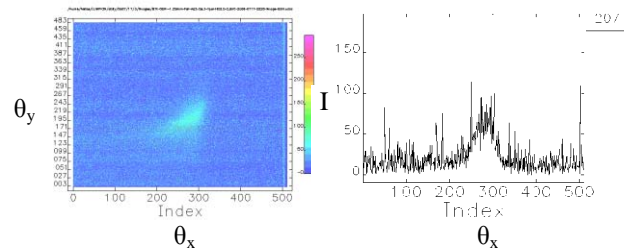

Figure 5: Vertically polarized far-field image of ODR with AQ2=29.3A (left) and the horizontal profile taken through the midpoint (right). The profile has a width of ~156 µrad (FWHM).
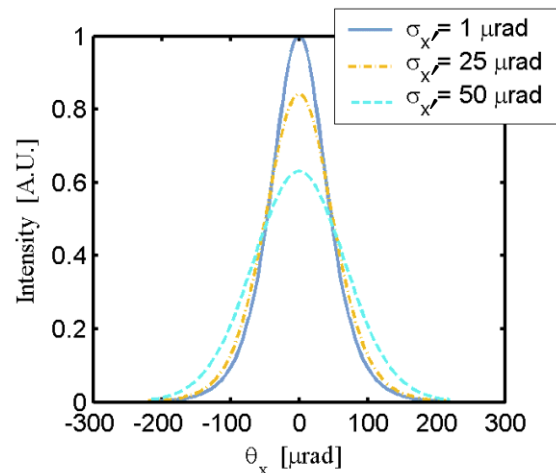

Figure 6: Calculation of the horizontal profile from the vertically polarized image for divergences of 1, 25, and 50 µrad. There is clear divergence sensitivity along the θ_x axis at $\theta_y = 0°$. The impact parameter was 1.25 mm.

SUMMARY

In summary, we have extended our investigations on imaging of the 7-GeV electron beam in the transport line of APS with both OTR and ODR. We have combined our near-field imaging results on beam size with our far-field imaging for divergence and trajectory angle information. By referencing our ODR results to the OTR results, we have obtained a better understanding of the use of the mechanism for an NI monitor.

ACKNOWLEDGEMENTS

REFERENCES

[1] Alex H. Lumpkin, NIM A557, 318 (2006).
[2] A.H. Lumpkin, W.J. Berg, N.S. Sereno, D.W. Rule, and C.Y. Yao, Phys. Rev. ST-AB, 10,022802 (2007).
[3] N.S. Sereno, private communication.
[4] T. Muto et al., Phys. Rev. Lett. 90(10), 104801-1 (2003).